Membrane Resonance and Stochastic Resonance Modulate Firing Patterns of Thalamocortical Neurons

Stefan Reinker[1], Ernest Puil[2], and Robert M. Miura[3]

[1] Department of Mathematics and
Institute of Mathematical Sciences
University of British Columbia, Vancouver, BC Canada V6T 1Z2

[2] Department of Pharmacology and Therapeutics
University of British Columbia, Vancouver, BC Canada V6T 1Z3

[3] Departments of Mathematical Sciences and
Biomedical Engineering and
Center for Applied Mathematics and Statistics
New Jersey Institute of Technology, Newark, NJ 07102 USA

CAMS Report 0203-23, Spring 2003

Center for Applied Mathematics and Statistics

NJIT

Editorial Manager(tm) JCNS
Manuscript Draft

Manuscript Number:

Title: Membrane Resonance and Stochastic Resonance Modulate Firing Patterns of Thalamocortical Neurons

Article Type: Manuscript

Keywords: Membrane resonance, stochastic resonance, thalami, neurons, neuron model, noise

Corresponding Author: Mr Stefan Reinker, Dipl.-Math. University of British Columbia

Other Authors: Ernie Puil, Robert M Miura

Membrane Resonance and Stochastic Resonance Modulate Firing Patterns of Thalamocortical Neurons

Stefan Reinker[1,2], Ernest Puil[3], and Robert M. Miura[1,2,4]

Department of Mathematics[1] and Institute of Applied Mathematics[2],
The University of British Columbia,
Vancouver, B.C Canada V6T 1Z2,
Department of Pharmacology & Therapeutics[3], The University of British Columbia,
Vancouver, B.C Canada V6T 1Z3,
and
Departments of Mathematical Sciences and Biomedical Engineering[4],
New Jersey Institute of Technology, Newark, NJ 07102, U.S.A.

Running Title:

Resonances in thalamocortical neurons

Address: Dr. Ernie Puil
Department of Pharmacology & Therapeutics
2176 Health Sciences Mall
The University of British Columbia
Vancouver, BC Canada V6T 1Z3

E-mail:puil@neuro.pharmacology.ubc.ca

Abstract

We examined the interactions of subthreshold membrane resonance and stochastic resonance using whole-cell patch clamp recordings in thalamocortical neurons of rat brain slices, as well as with a Hodgkin-Huxley-type mathematical model of thalamocortical neurons. The neurons exhibited the subthreshold resonance when stimulated with small amplitude sine wave currents of varying frequency, and stochastic resonance when noise was added to sine wave inputs. Stochastic resonance was manifest as a maximum in signal-to-noise ratio of output response to subthreshold periodic input combined with noise. Stochastic resonance in conjunction with subthreshold resonance resulted in action potential patterns that showed frequency selectivity for periodic inputs. Stochastic resonance was maximal near subthreshold resonance frequency and a high noise level was required for detection of high frequency signals. We speculate that combined membrane and stochastic resonances have physiological utility in coupling synaptic activity to preferred firing frequency and in network synchronization under noise.

Keywords: Membrane resonance, stochastic resonance, thalamic neurons, neuron model, noise.

1. Introduction

Many types of membrane interactions occur in central nervous system (CNS) neurons, affecting their ability to convert synaptic inputs into trains of action potentials. A combination of electrical properties confers an increased voltage response (membrane resonance) in a preferred range of input current frequencies. In thalamocortical neurons, a low threshold Ca^{2+} current, I_T, interacts with the passive membrane electrical properties to produce this membrane resonance (Hutcheon et al., 1994; Puil et al., 1994). Membrane resonance (or "I_T-resonance") can selectively amplify subthreshold periodic inputs and participate in rhythmogenesis (Hutcheon and Yarom, 2000). As previously, we refer to this preferred transformation of input signals, as frequency preference.

Noise from various sources also can influence, even increase, the conversion of inputs into action potential trains at specific frequencies (reviewed by Moss et al., 1994; Gammaitoni et al., 1998). This process, called stochastic resonance (SR), is independent from membrane resonance. SR appears as a maximum coherence between a subthreshold input and the stochastic response, measured by signal-to-noise ratio (SNR). At this optimal noise level, signal transmission improves, facilitating the detection of periodic inputs, as demonstrated in auditory hair cells (Jaramillo, 1998) and cold receptors (Longtin, 1996).

CNS neurons experience periodic current inputs during conscious and sleep states (Steriade et al., 1997). The main sources of noise in CNS neurons include spontaneous action potential firing, synaptic bombardment, spontaneous, miniature potentials due to neurotransmitter actions at receptor channels, and membrane noise arising from stochastic channel openings and closings (Destexhe et al., 2001; Steinmetz et al., 2000; Tuckwell, 1989). A phenomenon like SR occurs in

neurons of neocortical slices and hippocampal models (Rudolph and Destexhe 2001; Stacey and Durand, 2002).

In synergy, membrane resonance and SR may boost inputs and evoke qualitative changes in the firing response of neurons. This occurs in shark electroreceptors where SR interacts with subthreshold membrane currents to influence the coding of input signals (Braun et al., 1994). Without SR, membrane resonance due to I_T increases voltage responses with frequency content near the resonant frequency in thalamocortical neurons at subthreshold potentials. This amplification diminishes as the membrane potential approaches threshold (Hutcheon et al., 1994). Without membrane resonance, noise amplifies small subthreshold signals, which may cross threshold and lead to action potentials near the peaks of the input signal. Hence, interacting subthreshold and stochastic resonances may modulate the firing patterns of CNS neurons. We examined this possibility by determining the frequency dependence of SR in thalamocortical neurons of *in vitro* slices and in a Hodgkin-Huxley (HH)-type model.

We also have investigated the interactions of membrane resonance and SR by performing noise and sine wave stimulation and whole-cell patch clamp recordings in rat thalamocortical neurons. *In vitro* slice experiments are not conducive to stable recordings over long time periods, limiting the collection of statistical data for SR studies. A comparison of data obtained from different neurons also is difficult because of differing membrane properties. In such cases, a mathematical modelling approach is useful in providing simulated statistical SR data for comparison with the experimental results. We complement the experimental studies by employing computer simulations and analysis methods using an HH-model of thalamocortical neurons (Huguenard and McCormick, 1992; see also Hutcheon et al., 1996).

2. Methods

2.1 Slice preparation

We prepared thalamic slices, as previously described in detail (Tennigkeit et al., 1996). In brief, coronal slices (thickness, 400 μm) were sectioned with a Vibroslicer (Campden Instruments, London UK) from brain of Sprague-Dawley-rats (P13–P15) that had been anesthetized with isoflurane. For ~2 h prior to recording, the slices were maintained in a holding chamber containing oxygenated artificial cerebrospinal fluid (ACSF) at 23-25 °C. The ACSF had the following composition in (mM): 124 NaCl, 4 KCl, 1.25 KH_2PO_4, 2 $CaCl_2$, 2 $MgCl_2$, 26 $NaHCO_3$, and 10 glucose. The pH of the ACSF, continuously saturated with 95% O_2:5% CO_2, was 7.4. For recording, a slice was transferred to a submersion-type chamber (~1 ml) and perfused with oxygenated (95% O_2:5% CO_2) ACSF at a flow rate of 1-2 ml/min.

2.2 Electrical recording

Whole-cell patch-clamp recordings were performed using an Axoclamp 2A amplifier in the current-clamp mode and pClamp software (version 8.1, Axon Instruments Inc., Foster City, CA, U.S.A.). Voltage and current measurements were sampled at 20 kHz with an anti-aliasing filter (time constant, 0.2 μs), and with the output bandwidth of 30 kHz. The recording electrodes were prepared from borosilicate glass (1.5 mm OD, WPI Instruments, Tokyo, Japan), using a micropipette puller (Model PP-81, Narishige Instruments, Tokyo, Japan). The pipettes were filled with a solution containing (in mM): 140 K-gluconate, 10 ethylene-glycol-bis-(β-aminoethyl ether)-N,N,N′,N′-tetraacetic acid (EGTA), 5 KCl, 4 NaCl, 3 $MgCl_2$, 10 N-[2-hydroxyethyl] piperazine-N′-[2-ethansulfonic acid] (HEPES, free acid), 1 $CaCl_2$, 3 Na_2·ATP, and 0.3 Na·GTP. Equilibration of

this solution with 10% gluconic acid resulted in a pH of 7.4. The electrode resistances ranged between 6 and 10 MΩ.

The medial geniculate body (MGB) was identified by using differential interference contrast (DIC) microscopy and infrared (IR) illumination (Axioskop, Zeiss Instruments, Jena, Germany) with an IR-sensitive video camera (Hamamatsu, Tokyo Japan). Whole-cell measurements were conducted on visually selected neurons in the ventral portion of the MGB (23-25°C). The use of sine waves and swept sine wave (ZAP) inputs for current injection into neurons and the Reactive Current Clamp (RCC) have been described previously for testing the frequency responses in neurons as well as in the model (Hutcheon et al., 1996; Puil et al., 1994). The RCC is a general technique for interactively coupling a computer algorithm to a neuron. Here, we used the RCC only to inject background noise and computer generated inputs into a neuron. With the RCC, Gaussian white noise, which was generated using a Box-Mueller algorithm, was injected into the neuron at a rate of 8 kHz. A potential of 11 mV was subtracted from the voltage measurements to compensate for the junction between the ACSF and electrode solution (Tennigkeit et al., 1996). The experimental data were analyzed offline using Clampfit 8 software.

2.3 The Huguenard-McCormick Model

We used a HH-type system of equations for modeling thalamocortical neurons.

$$C_m \frac{dV_m}{dt} = -\sum I_{ion} + I_0 + I_{signal}(t)$$

where I_{ion} includes Na^+ (I_{Na}), K^+ (I_C), and T-type Ca^{2+} (I_T) currents, as described by Huguenard and McCormick (1992) and with minor modifications by Hutcheon et al. (1994). The model is capable

of producing tonic and burst firing and subthreshold resonance similar to thalamocortical neurons. To test the response of this model to current inputs, we used sine waves, $I_{signal}(t) = A \sin(\omega t)$ with frequency $f = \omega/2\pi$, and swept sine waves, $I_{signal}(t) = A \sin(\omega t^b)$ or "ZAP function" (Hutcheon et al., 1994).

In order to model a stochastic background current, a stochastic term $\eta(t)$ was added to a constant background current i_0,

$$I_0 = i_0 + \eta(t).$$

We assumed that noise autocorrelation times were short compared to the system's dynamics and chose Gaussian white noise with strength σ for $\eta(t)$. That is, the autocorrelation of η is proportional to a delta function, $\langle \eta(t), \eta(t') \rangle = \sigma \delta(t-t')$. The stochastic equations were simulated using a fourth order Runge-Kutta algorithm (Kloeden and Platen, 1992) for stochastic differential equations. Again, Gaussian white noise was generated with the Box-Mueller algorithm. The stepsize used in the computations was 0.01 s, which proved to be small enough to give statistically stable results. All simulations were programmed in C (Gnu C-compiler) and run on a PII/550 Linux PC.

2.4 Impedance Analysis

The subthreshold frequency dependent voltage response to input currents can be measured easily with a swept sine wave signal (Hutcheon et al., 1994, Puil et al., 1994). The impedance (Z) at frequency ω and resting voltage V_0 can be computed from the ratio of Fourier transforms of voltage response and current input

$$Z(\omega, V_0) = \frac{FT(V; V_0)}{FT(I; V_0)}$$

where V and I are the voltage and current traces, respectively, and FT denotes the Fourier transform. Then, the absolute value of the impedance, |Z|, describes the magnitude of the voltage response relative to small sine wave inputs and a preferred or resonant frequency appears as maximum impedance. Fourier transforms were computed with the built-in functions of Matlab.

2.4 Analysis of the spike train

The occurrence of the action potential was defined when V depolarized through 0 mV. We used the interspike intervals histogram (ISIH) to illustrate the firing characteristics. Stochastic resonance is normally investigated with inputs that are a combination of subthreshold sine waves and noise and demonstrated through statistical analysis of transitions between different states in the dynamical system. In neurons, such a transition occurs when the neuron fires an action potential in response to the input signal current and noise.

Using different noise amplitudes (σ) and sine wave inputs at different frequencies (f), we recorded from a neuron for 40-80 s in each run, in order to obtain a sufficient number of action potentials for statistical analysis of the firing pattern. We identified the occurrences of the action potentials with a Poincaré map (Schmidt trigger) when the membrane voltage V_m crossed 0 mV, with a positive slope. The resulting spike train was used to plot an ISIH using Matlab. ISIHs typically have multiple peaks, and the area under the peak at the input frequency is a measure of how much of the input frequency is present in the output spike train. Consequently, we define

$$SNR = 10\log_{10}\left(\frac{\#\ of\ spikes\ near\ input\ \ period}{total\ \#\ of\ spikes}\right)$$

as an estimate of the correlation between the periodic input signal and output spike train. This method, similar to that of Longtin et al. (1991) and Douglass et al. (1993), filters out the contributions from the higher order peaks, allowing an isolation of the response at the input frequency. For SR, SNR goes through a maximum for increasing noise level.

3. RESULTS

3.1 Experimental Results

ZAP Function Stimulation We used the ZAP function to test the frequency responses in MGB neurons. Figure 1A shows that the amplitude of the subthreshold voltage response varied with frequency in a neuron held at -70 mV. Figure 1B shows the corresponding impedance magnitude curve with one maximum at ~2 Hz. Hence, neurons at subthreshold potentials exhibited resonance as a frequency preference for inputs near 2 Hz. Depolarization of neurons from rest (~-70 mV) to near threshold diminished the resonance at -55 mV. This confirmed the observations of Tennigkeit et al. (1997).

Sine Wave Stimulation with Noise The application of a subthreshold sinusoidal current input with white noise to a neuron near -70 mV evoked action potentials, most often near the peak of the voltage response (Fig. 2). However, not every sine wave peak elicited an action potential, and the output of the neuron exhibited a stochastic firing pattern that depended on the sine wave input frequency.

The ISIH resulting from the noisy sine wave input had a multi-peaked distribution. Figure 3 shows ISIHs for different values of σ and f. The first peak of each ISIH was near zero interspike interval time, and resulted from multiple action potentials at the top of one sine wave maximum. The second ISIH peak occurred at an interspike interval time that was roughly equal to the period of the input sine wave, and thus, corresponds to action potentials on consecutive maxima of the input. More peaks in the ISIH appear at integer multiples of the period and correspond to one or more intervening sine wave maxima without action potentials (cf. Figs. 2, 3B).

The interspike interval distribution depended on the noise level and sine wave frequency of the combined input. At low noise levels, action potentials frequently did not occur on sine wave maxima (Fig. 3A). Consequently, the ISIH peaks at multiples of sine wave period were large whereas the peak was relatively small at the input period (1000 ms). More action potentials occurred at higher, intermediate noise levels (Fig. 3B), resulting in relatively small peaks at higher multiples of the input period. The ISIH peak at 1000 ms increased because the greater noise amplitude evoked action potentials on almost every sine wave peak. A greater number of action potentials occurred at high noise levels (Fig. 3C), even when the input sine wave signal was not near its peak. Often, bursts of two or more action potentials occurred on a peak, resulting in interspike interval events at less than the period of the sine wave signal. The peak in the ISIH at the input period moved to lower interspike times due to discharges that did not coincide with the peaks of the input signal. A sine wave current input at a different frequency shifted the ISIH peaks at multiples of the input period (Fig. 3D).

The evolution of the ISIH showed a progression of SR as a function of noise level (Fig. 3A-C). The ISIH peak at the input period was the largest relative to the other peaks when the noise was at an intermediate level. The SNR, shown in Fig. 4A, also went through a maximum at these noise

levels. Since the probability of crossing threshold was low at low noise levels, the number of action potentials was too small for a good correlation with the input signal, leading to a small SNR. At high noise levels, the firing probability was too high, resulting in extraneous action potentials. This implied that the neuron was discharging in response to the noise level, and not to the sine wave stimulation. The SNR was small at high noise levels, as observed at low noise levels. The typical SNR shape shown in Fig. 4A demonstrates that noise can increase signal detection over a certain frequency range in thalamocortical neurons. The occurrence of an optimal noise level with a maximal presence of the input frequency in the output train is the hallmark of SR.

The SNR depended on input frequency, as well as noise level. This is evident in Fig. 4B, which shows that the SNR is high between 1 and 3 Hz and is smaller for higher and lower frequencies. This represented a maximal coherence between the sinusoidal current input and the output spike train at the input frequency. The SR was in the same frequency range, but was less pronounced than the subthreshold resonance.

3.2 Modelling Results

Impedance Analysis Mathematical analysis of the model for I_T-resonance subjected to oscillatory inputs yields the small signal impedance with a response that is dependent on the voltage and input frequency (Hutcheon *et al*., 1994),

$$Z(\omega, V) = \left[\mathrm{abs}\left(g_{leak} + iC_m\omega + g_T m_{T0}(V)^2 h_{T0}(V)\left(2\frac{m'_{T0}(V)}{m_{T0}(V)}\ \frac{1}{1+i\omega\tau_{mT}(V)} + \frac{h'_{T0}(V)}{h_{T0}(V)}\ \frac{1}{1+i\omega\tau_{hT}(V)} + \frac{1}{V-V_{Ca}} \right)(V-V_{Ca}) \right) \right]^{-1}.$$

A three-dimensional graph of the impedance magnitude of this function (Fig. 5) shows its dependence on input frequency and resting potential. The subthreshold impedance is maximal at 3

Hz and -70 mV and is smaller for higher and lower voltages, as well as for higher and lower frequencies. A frequency preference to small signals with components near 3 Hz is present near the resting potentials. When the membrane potential approaches the threshold for an action potential, resonance diminishes, resulting in a flat frequency response. The disappearance of resonance prompted the question whether I_T resonance would influence the firing behavior of thalamocortical neurons. Impedance is defined for small inputs in the linear regime whereas nonlinear dynamics, such as the activation of channels, render "impedance" a meaningless concept for larger inputs. Hence, a subthreshold resonance, even near the threshold for action potentials, may not translate into a preferred firing frequency.

Sine Wave and Noise Stimulation The SNR of the model can be calculated in the same way as above for experimental data. Figure 6A shows a three-dimensional graph of SNR and its dependence on noise level and input frequency, obtained from simulations for long time periods (100,000 s). Each point in the graph was calculated from an ISIH for a particular combination of noise and frequency. At fixed input frequency (parallel to the σ-axis) and varying noise levels, the curve had a typical SR shape with one SNR maximum at an intermediate noise level. Thus, the model exhibited SR similar to that observed in the experiments.

At each fixed noise level (parallel to the f-axis), the SNR also had a maximum which is visible in the contour plot of SNR (Fig. 6B). The absolute maximum of SNR was obtained at $\sigma = 0.2$ nA and $f = 1.75$ Hz. The optimal noise level was lower at this frequency than at higher or lower frequencies (Fig. 6B). This constitutes a preferred SR frequency of the model. The noise level required for optimal detection (denoted by the thick curve in Fig. 6B) increased for higher frequencies. This frequency preference was absent when $g_T = 0$, that is, in a model without I_T and

resonance (Fig. 6C). In the non-resonant model, the optimal noise level increased with input frequency. When compared to Figure 6A and B, this shows that the preferred frequency was dependent on I_T. In summary, a frequency- and noise-dependent SR was present in the model.

4. Discussion

4.1 Experiments

The present experiments demonstrate the occurrence of stochastic resonance in thalamocortical neurons as a maximum in SNR that depended on the noise level. This was evident from interspike interval histograms, showing the effects of combined noise and subthreshold periodic signal inputs on the spike train output. SR in thalamocortical neurons depended on the frequency of the periodic subthreshold current input signal and exhibited a broad frequency preference for periodic inputs between 1 and 3 Hz. Although SR occurs in sensory cells (Douglass et al., 1993; Braun et al., 1994; Jaramillo et al., 1998; Longtin et al., 1996) and neocortical neurons (Rudolph et al., 2001), this is the first report of frequency preference of SR in excitable cells.

4.2 Modelling

Simulations of the Huguenard-McCormick equations showed that SR in the model was consistent with the experimental findings. SR was apparent in the model at input frequencies between 0.5 and 6 Hz, from the typical SNR shape with one maximum for changing noise level. The optimal noise level depended on signal frequency, with high frequencies requiring high noise levels, as observed in a double well system (Berdichevsky et al., 1996) and neuron models (Reinker et al., 2003; Baltanas et al., 2002). Massanes et al. (1999) explained frequency dependence of SR on the basis that high frequency inputs have less likelihood, per period, to evoke an action potential on a signal

peak because of their short period and hence, less time near threshold. Since one action potential on top of each signal peak is needed for optimal detection, i.e., a maximal SNR, more noise is necessary at higher frequencies for the voltage to cross threshold in the briefer time (Fig. 6B,C; cf. Gammaitoni, 1998). Consequently, the change in preferred frequency of SR arises from the interaction of the signal period with the neuron's firing probability during a signal period.

4.3 Comparison of experiments and model

We observed subthreshold and stochastic resonance phenomena in experiments and the model. The present studies confirm, for MGB neurons, the similarity of subthreshold resonance in the I_T model (Hutcheon et al., 1994) to the I_T-resonance as observed in mediodorsal thalamic neurons (Puil et al., 1994). In SR, the actual SNR levels were higher in experiments than in the model, implying that neurons fire less reliably in the model. A possible explanation for the increased reliability in real neurons is that the injected noise was not close to the site for action potential generation. Between the microelectrode tip and axon hillock, high-frequency filtering by the membrane may have altered the spectral content of the noise. Consequently, the effective noise level at the axon hillock would be lower than at the point of noise injection into a neuron. In contrast, the equations model a point neuron without any spatial attenuation.

The SR was frequency dependent in experiment and model. The preferred frequency of SR in the neuron occurred in the range of 1 to 3 Hz, whereas the model had a more sharply defined preferred frequency near 1.75 Hz. The optimal noise level also depended on the input frequency in a range between 0.5 and 6 Hz. We observed a similar dependence of the preferred firing frequency on noise injected into the resonant Hindmarsh-Rose model of the bursting neuron (Reinker et al., 2003; see also Wu et al., 2001).

We demonstrated that the frequency dependence of SR resulted from subthreshold I_T-resonance which diminished on depolarization to near threshold. The I_T-resonance amplified input signals at preferred frequencies which noise boosted above this threshold. Because of this boosting, the highest firing probability occurred near the peaks of the sine wave signal. The preferred frequency of SR depended on the noise level but was in the same preferred frequency range as the subthreshold resonance. Compared to the cell bodies, the dendrites generate more low threshold calcium current which is instrumental for producing subthreshold resonance (Destexhe et al., 1998). The dendrites also receive the majority of excitatory postsynaptic potential (EPSP) inputs. The juxtaposition of I_T-resonance and SR between dendritic and axon hillock sites may have physiological utility in EPSP-action potential coupling.

A limitation of our studies is the use of Gaussian white noise which ignores autocorrelation in the noise. Godivier and Chapeau-Blonde (1996) showed that noise from multiple random synaptic inputs exhibits SR in neuron models. Long noise autocorrelation times of the order of one-tenth of a second can interfere with the membrane time scale of the model and alter SR. When the noise autocorrelation time is much shorter than the resonance time scale, however, the noise autocorrelation has negligible influence on resonance (Hänggi et al., 1993). In our studies, the period of the resonant frequencies ranged in seconds, justifying the use of uncorrelated white noise.

A connection between SR and frequency preference has additional consequences for thalamocortical neuron function. In the context of a neuron receiving EPSP inputs, the effect of noise on the preferred frequency arising from the subthreshold membrane resonance constitutes an ability to modulate the output frequency. Noise change will change resonance. The noise change may result from the opening or closing of membrane ion channels in small populations, a source of membrane noise (Steinmetz et al., 2000). In a stochastic neural network, switching between states

of network activity may occur when noise changes the preferred frequency of neurons. Periodic inputs to neurons generated by oscillations in large scale networks are common features in the brain (Steriade et al., 2000). Similar to our simulations with sine wave inputs, network oscillations result in synchronized synaptic events. In the cortico-thalamocortical network that generates oscillations (Steriade et al., 1997), the preferred frequencies for SR in neurons would amplify input action potential trains that arrive at the matching frequency. This would promote synchronization which is critical for conscious behavior and sleep states. Our experiments and the model were at room temperature. In mammalian neurons, the time constants of membrane ion currents would be shorter, resulting in a higher resonance frequency. A connection is plausible between the SR frequency preference and the strong 5 Hz frequency component in brain activity. Increased synchronization based on combined membrane resonance and SR may facilitate generalized *absence* seizures, a condition when the cortico-thalamocortical system displays increased synchronization and disrupted brain function (Bal et al., 2000).

In summary, we have demonstrated stochastic resonance in association with the preferred firing frequency of thalamocortical neurons and in the Huguenard-McCormick neuron model. The preferred frequency of SR resulted from a subthreshold membrane resonance. This I_T-resonance enables the neuron to select and amplify inputs at the resonant frequencies. Then, the addition of white noise current can induce neuronal firing with a preferred frequency that stems from the membrane resonance in the stochastic output spike train. The frequency dependence of the optimal noise level may have significance for synaptic integration and rhythmogenesis in a noisy environment. Thus, noise intensity may act as a control parameter for information processing reliability.

Acknowledgements

We gratefully acknowledge financial grant support from the University of British Columbia for the University Graduate Fellowship to Mr. S. Reinker, the Natural Sciences and Engineering Research Council of Canada to Dr. R.M. Miura, and the Canadian Institutes for Health Research, as well as the Jean Templeton Hugill Chair in Anesthesia to Dr. E. Puil.

References

Bal T, Debay D, Destexhe A (2000) Cortical feedback controls the frequency and synchrony of oscillations in the visual thalamus. Journal of Neuroscience 20: 7478-7488.

Baltanas JP, Casado JM (2002) Noise-induced resonances in the Hindmarsh-Rose neuronal model. Physical Review E 65: 041915.

Berdichevsky V, Gitterman M (1996) Stochastic resonance in a bistable piecewise potential: analytical solution. Journal of Physics A 29: L447-L452.

Braun HA, Wissing H, Schäfer K, Hirsch MC (1994) Oscillation and noise determine signal transduction in shark multimodal sensory cells. Nature 367: 270-273.

Destexhe A, Rudolph M, Fellous JM, Sejnowski TJ (2001) Fluctuating synaptic conductances recreate in vivo-like activity in neocortical neurons. Neuroscience 107: 13-24.

Douglass JK, Wilkens L, Pantazelou E, Moss F (1993) Noise enhancement of information transfer in crayfish mechanoreceptors by stochastic resonance. Nature 365: 337-340.

Gammaitoni L, Hänggi P, Jung P, Marchesoni F (1998) Stochastic resonance. Reviews of Modern Physics 70: 223-287.

Hutcheon B, Miura RM, Yarom Y, Puil E (1994) Low-threshold calcium current and resonance in thalamic neurons: a model of frequency preference. Journal of Neurophysiology 71: 583-594.

Hutcheon B, Miura RM, Puil E (1996) Models of subthreshold membrane resonance in neocortical neurons. Journal of Neurophysiology 76: 698-714.

Hutcheon B, Yarom Y (2000) Resonance, oscillation, and the intrinsic frequency preferences of neurons. Trends in Neuroscience 23: 216-222.

Jaramillo F, Wiesenfeld K (1998) Mechanoelectrical transduction assisted by brownian motion: A role for noise in the auditory system. Nature Neuroscience 1: 384-388.

Kloeden PE, Platen E (1992) Numerical Solution of Stochastic Differential Equations, Berlin: Springer Verlag.

Longtin A, Bulsara A, Moss F (1991) Time-interval sequences in bistable systems and the noise-induced transmission of information by sensory neurons. Physical Review Letters 67: 656–659.

Longtin A, Hinzer K (1996) Encoding with bursting, subthreshold oscillations, and noise in mammalian cold receptors. Neural Computation 8: 215-255.

Massanes S, Vicente C (1999) Nonadiabatic resonances in a noisy FitzHugh-Nagumo neuron model. Physical Review E 59, 4490-4497.

McCormick DA, Huguenard JR (1992) A model of the electrophysiological properties of thalamocortical relay neurons. Journal of Neurophysiology 68: 1384-1400.

Moss F, Pierson D, O'Gorman D (1994) Stochastic resonance: tutorial and update. International Journal of Bifurcation and Chaos in Applied Sciences and Engineering 4: 1383-1397.

Press WH (1992) Numerical Recipes in C: The Art of Scientific Computing, New York: Cambridge University Press.

Puil E, Meiri H, Yarom Y (1994) Resonant behavior and frequency preference of thalamic neurons. Journal of Neurophysiology 71: 575-582.

Reinker S, Puil E, Miura RM Stochastic and suprathreshold resonances in a stochastic Hindmarsh-Rose model of thalamic neurons. Bulletin of Mathematical Biology, submitted.

Rudolph M, Destexhe A (2001) Do neocortical pyramidal neurons display stochastic resonance? Journal of Computational Neuroscience 11: 19-42.

Stacey WC, Durand DM (2000) Stochastic resonance improves signal detection in hippocampal CA1 neurons. Journal of Neurophysiology 83: 1394-1402.

Steinmetz PN, Manwani A, Koch C, London M, Segev I (2000) Subthreshold voltage noise due to channel fluctuations in active neuronal membranes. Journal of Computational Neuroscience 9: 133-48.

Steriade M (2000) Corticothalamic resonance, states of vigilance and mentation. Neuroscience 101: 243-276.

Steriade M, McCormick DA, Sejnowski TJ (1993) Thalamocortical oscillations in the sleeping and aroused brain. Science 262: 679-685.

Tennigkeit F, Ries CR, Schwarz DWF, Puil E (1997) Isoflurane attenuates resonant responses of auditory thalamic neurons. Journal of Neurophysiology 78: 591-596.

Tuckwell HC (1989) Stochastic Processes in the Neurosciences, CBMS-NSF Regional Conference Series in Applied Mathematics 56, Philadelphia PA: SIAM.

Wu S, Ren W, Kaifen H, Huang Z (2001) Burst and coherence resonance in the Rose-Hindmarsh model induced by additive noise. Physics Letters A 279: 347-354.

FIGURE LEGENDS

Figure 1. Subthreshold voltage response of MGB neuron to swept sine wave stimulation. **A:** Constant amplitude current (0.1-10 Hz) input evoked voltage response of non-uniform amplitude. **B:** Frequency dependence of impedance calculated from A showed maximum impedance near 3 Hz, demonstrating a frequency selectivity for inputs. Neuron held with DC at -70 mV (upper record) and at -55 mV (lower record) showed diminished resonance on depolarization.

Figure 2. Voltage record, V_m, from MGB neuron under subthreshold sine wave (1 Hz) and noise stimulation. The combined current input led to stochastic firing, most likely on the peaks of the sine wave signal. Multiple action potentials on a single peak or skipping of signal peaks occurred.

Figure 3. Interspike interval histogram distributions show dependence on input noise level (σ) and sine wave frequency (f). The ISIHs were computed from membrane potential recordings of long duration (**A**, 67 s; **B**, 76 s; **C**, 55 s; and **D**, 75 s).

Figure 4. Signal to noise ratio (SNR) computed from interspike interval histograms obtained from the experiments in Figure 3. **A:** SNR dependence on noise strength for an input frequency of 1 Hz. The curve shows one maximum at an intermediate noise level and declines for higher and lower noise levels. This shape is typical for stochastic resonance. **B:** SNR dependence on input frequency for fixed noise input with an amplitude of 0.6 nA. The SNR curve shows a broad

maximum between 1 and 3 Hz. This frequency preference of stochastic resonance is similar to the subthreshold resonance in Figure 1, but it appears in the action potential pattern.

Figure 5. Impedance diagram of Huguenard-McCormick model. 3-D plot of impedance magnitude, resting membrane potential, V_m, and signal frequency, f, obtained from the analytic equation for the impedance. The peak at V_m = -70 mV, f = 3 Hz signifies a maximum response to inputs at this frequency. As V_m approaches the firing threshold (at ~-50 mV), the membrane resonance is reduced.

Figure 6. **A:** Signal to noise ratio (SNR) as computed from the Huguenard-McCormick model, depended on noise level and input frequency. For each fixed frequency, the SNR has the typical SR shape with one maximum. The location of maximum SNR depended both on input frequency and noise level, with the absolute maximum (denoted by an *) attained at 1.75 Hz and 0.2 nA. **B:** Contour plot, derived from A, of the SNR dependence on noise level and input frequency. For each frequency, the typical stochastic resonance curve has one maximum along the σ-axis. The thick line denotes the frequency of maximum SNR for each noise level used in the simulations. In general, a higher input frequency needed higher noise level for optimal detection. Only at f = 1.75 Hz a lower noise level was optimal than the required noise for higher and lower frequencies. **C:** Contour plot of the SNR dependence on noise level and input frequency for the model without I_T-resonance, that is $g_T = 0$. There was stochastic resonance for every input frequency. The optimal noise level increased monotonically with the frequency.

Figure 1, single col

Click here to download high resolution image

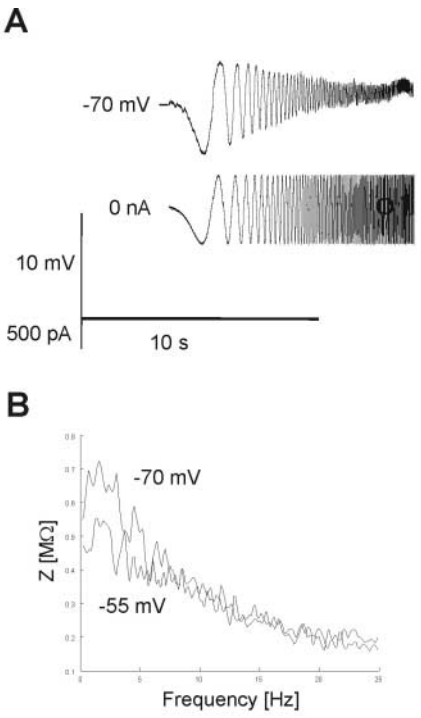

Figure 2, single col

Click here to download high resolution image

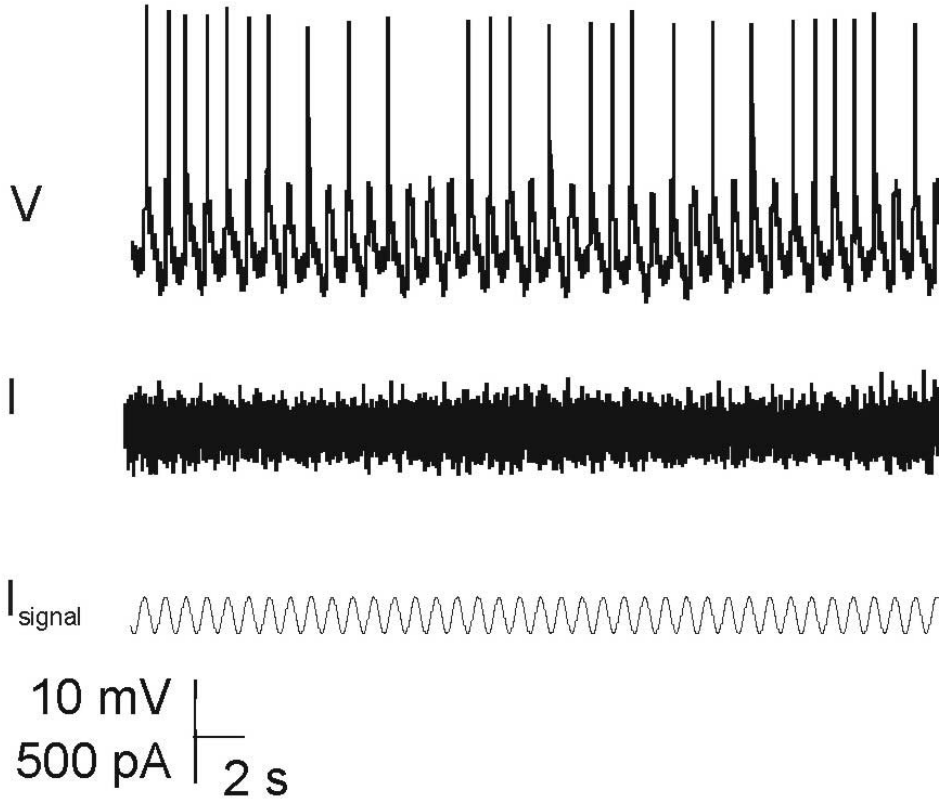

Figure 3, double col

Click here to download high resolution image

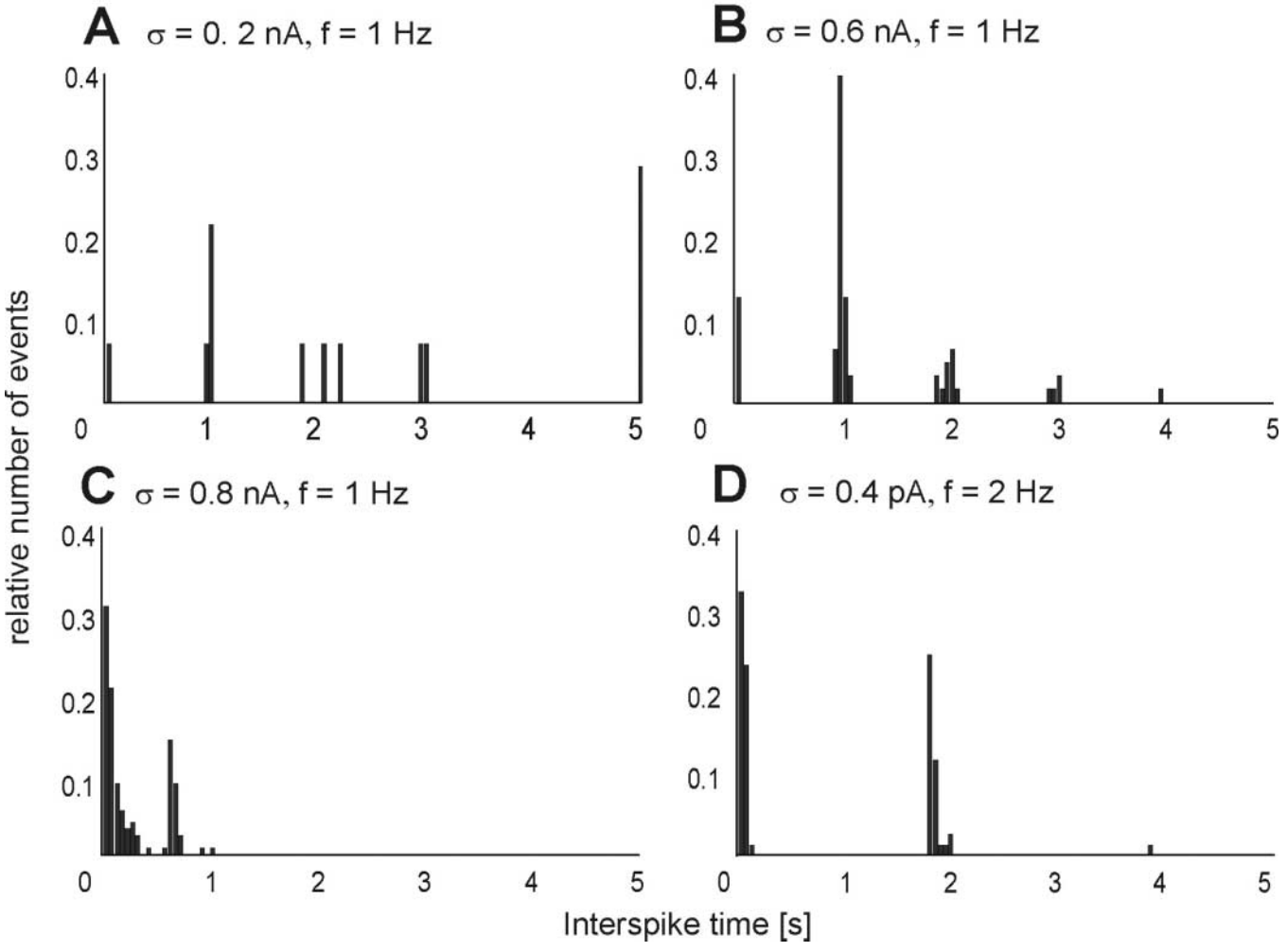

Figure 4, single col

Click here to download high resolution image

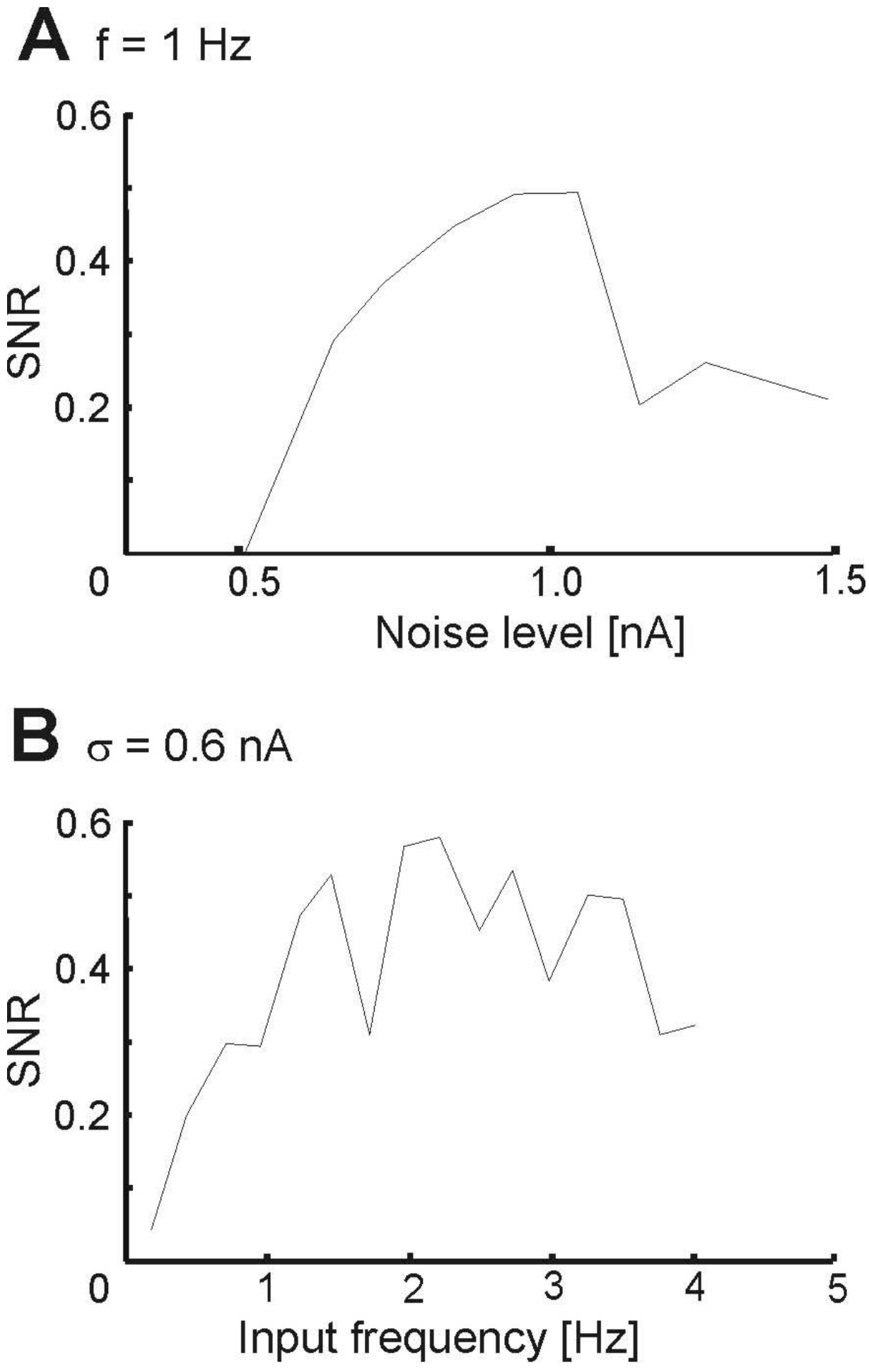

Figure 5, single col

Click here to download high resolution image

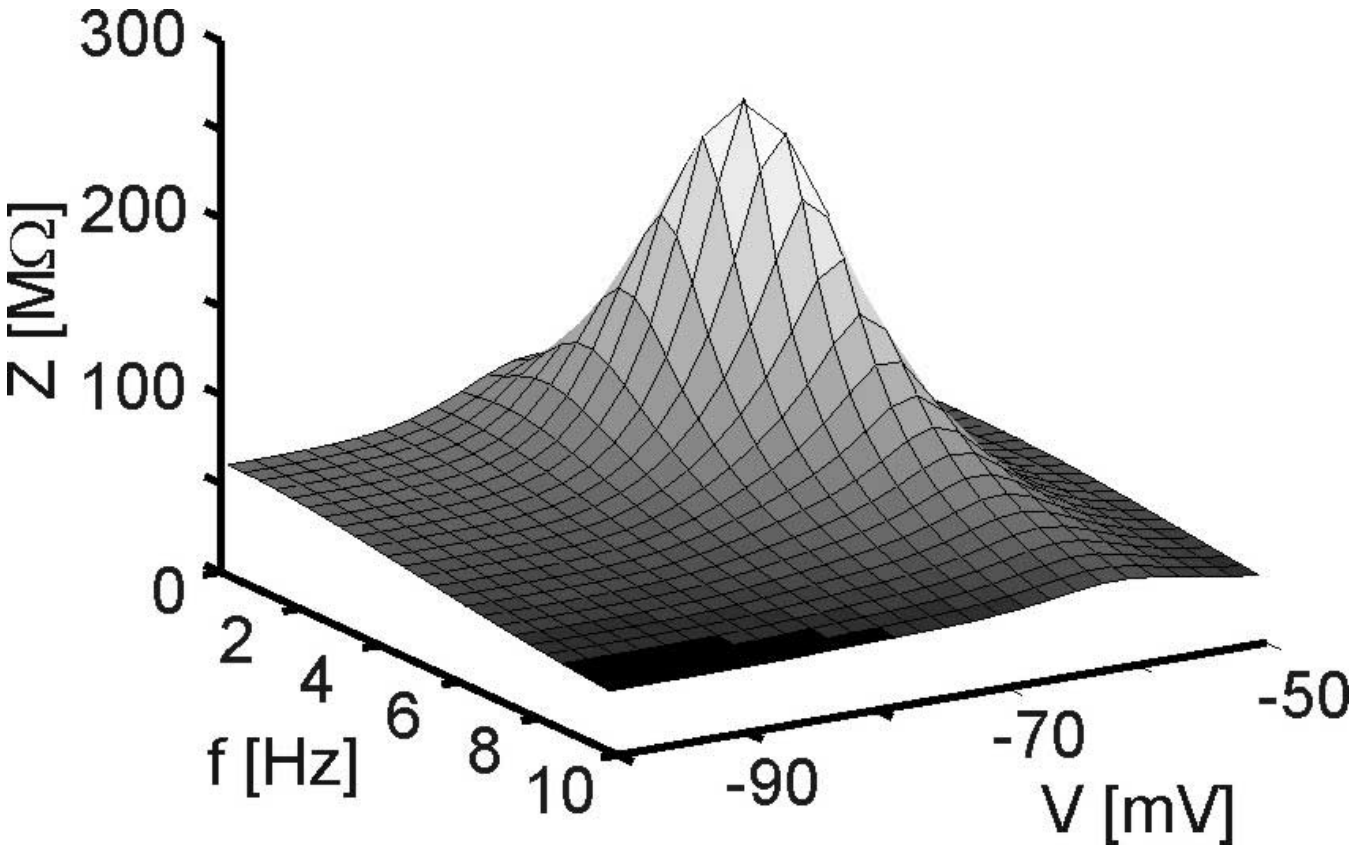

Figure 6, single col

Click here to download high resolution image